PROCEEDINGS, 50th Workshop on Geothermal Reservoir Engineering
Stanford University, Stanford, California, February 10-12, 2025
SGP-TR-229

Importance of linkage zones for geothermal exploration in the Rio Grande Rift (Española and Santo Domingo basins, New Mexico): contribution of analogue modelling

Nicolas Dall'asta[1], Yoann Denèle[2], Vincent Regard[2], Delphine Rouby[2], Anne Frayssignes[2], Mael Derian[2], Stephane Bonnet[2], Bastien Hermant[1]

[1]TLS-GEOTHERMICS- 91 Chemin de Gabardie, 31500, Toulouse, FRANCE

nicolas.dallasta@tls-geothermics.com

[2]GET, Université de Toulouse, CNRS, UPS, IRD, CNES, 14 av. E. Belin, F-31400 Toulouse, France

Keywords: Linkage zones, Rio Grande rift, Analogue modelling, Hydrothermal circulations, Geothermal exploration

ABSTRACT

Linkage zones are key structures in rift systems because they link rift segments at different scales. Linkage zones have various geometries depending on rift segments offset, the rheology of the lithosphere and structural or thermal inheritance. Linkage zones are also promising structures for geothermal exploration with complex structural settings resulting from significant strain rotation through time.

The Rio Grande rift system is an under-explored rift system with strong geothermal potential. The Española and Santo Domingo basins form a large linkage zone of the rift with a two-stage evolution: an initial distributed deformation phase, followed by a more localized deformation phase. The kinematic and structural evolution of this area remains nevertheless unclear.

To better understand this linkage zone, we combined physical modeling and a structural synthesis based on fault trajectories mapping by DEM analysis and slip-data from previous studies. We also focused on the role played by rheology throughout rifting, as well as the impact of inheritance on the linkage geometry. This approach allows us to better constrain the interactions between the different deformation structures in the Española Basin and the structural settings favorable for deep geothermal energy.

1. INTRODUCTION

Linkage zones are areas where two rift segments connect or overlap with each other. The evolution and structure of these linkage zones is complex and depends on various factors such as lithosphere rheology, but also the distance between rift segments and the rift obliquity (Zwaan and Schreurs, 2017; Dall'Asta et al., 2024). In other rift settings (e.g., the Tjörnes Fracture Zone in Iceland, Taupo rift in New Zealand or the Basin and Range in the US), the linkage zones are areas concentrating hydrothermal circulations and volcanic activity (Rowland and Sibson, 2004; Lupi et al., 2010; Faulds and Hinz, 2015).

The Rio Grande rift system offers a unique natural laboratory for studying the impact of linkage-fault systems in fluid circulation and magma transfer within the crust. Located within the intramountainous rift systems of the Colorado Plateau, which have been active since Late-Oligocene, the Rio Grande rift extends north-south along the eastern edge of the region. This rift system, spanning 30 to 80 kilometers in width, is narrow compared to the 800- kilometer- wide Basin and Range rift system in the Great Basin, even though both exhibit similar thermal properties. Notwithstanding its considerable geothermal potential, only a single geothermal power plant, Lightning Dock, is currently operational in the southern region where the Rio Grande rift converges with the Southern Basin and Range province. The Española and Santo Domingo basins, located along the Rio Grande rift north of Albuquerque, represent an example of a broad linkage zone. The role of structural inheritance in the localization of the rift segments and the orientation of the linkage zones is a key consideration to understand the evolution of the syn-rift basins. However, the evolution and kinematic processes of the rift remain poorly understood (see Liu et al., 2019 for a review). To address this knowledge gap, we use analogue modelling in combination with structural synthesis to better constrain the three-dimensional strain field through time. This work is complemented by a re-evaluation of crustal rheology throughout rift evolution using a synthesis of the volcanic evolution, as well as geophysical data and new data from lower crustal xenolith (Cipar et al., 2020).

The main questions addressed concern the structural evolution of the Española-Santo Domingo linkage throughout rifting and the role of rheology on its evolution. Based on the Rio Grande example, we also discuss the impact of the linkage structures on the fluid transfer in the crust.

2. GEOLOGICAL CONTEXT

The Rio Grande is an Oligo-Miocene to present-day rift affecting the southern Rocky Mountains (Olsen et al., 1987; Chapin et al., 1994; Ricketts et al., 2016). It is a narrow rift system, 30 to 80 km wide, characterized by high elevations, with basin altitudes decreasing from north to south, ranging from 2000 m to 1300 m, despite significant extension (17% to 50%; Russell and Snelson, 1994). It is mainly N-S trending between two tectonically stable blocks, the Colorado Plateau and the Great Plain area and connecting to the south with the Southern Basin and Range (Fig. 1).

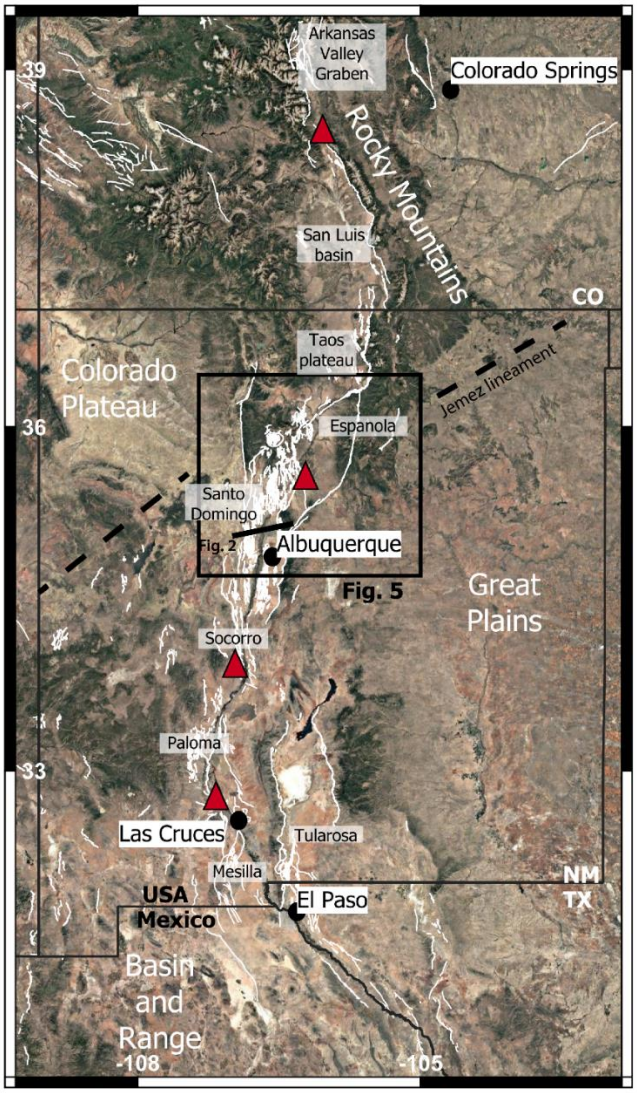

Figure 1: Map of the Rio Grande rift system from Colorado to Texas. The names of the main basins along the rift as well as the main tectonic provinces are indicated. The red triangles highlight the main linkage zones. The NE-SW Jemez lineament corresponds to a Cenozoic to Quaternary volcanic alignment localized along a Proterozoic suture between the Yavapai and Mazatzal terranes (Daniel et al., 1995).

The Rio Grande rifting event underwent a two-stage evolution characterized by early rift basins formed at the top of low-angle normal fault systems, intersected by high-angle boundary faults (Morgan et al., 1986). The early structures are locally observed at the surface on the current rift shoulders, such as in the Sandia Mountains northwest of Albuquerque (Ricketts et al., 2016). This sequential evolution led to specific structural characteristics of the basin, particularly in the Albuquerque basin. This includes structural benches and embayments (Hagan and Santa Fe embayments), which both represent an earlier alternation of structural highs and basins along the rift segment tip lines. Upper-crustal cross-sections of the Albuquerque basin derived from seismic interpretations highlight the thermo-mechanic evolution of the rift (Fig. 2), compared to thermal characteristics based on granulite xenolith data (Cipar et al., 2020).The first stage of rift evolution, from the Oligocene to the early Miocene, is characterized by distributed deformation and a shallow décollement level, which we interpret as corresponding to the brittle-ductile transition (approximately 5 km depth) within a warm crust (with a Moho temperature of about 1000°C).The second rift stage, from the Late Miocene to the present, is characterized by localization of deformation on a high-angle normal fault system, leading to deeper, narrower late-rift basin (Fig. 2). The decollement level is deeper than the first rift stage (around 10 km) within a cooler continental crust (Fig. 2).

The Lithosphere-asthenosphere Boundary (LAB) is located at 80km depth (Hansen et al., 2015). The Moho is at ca. 35-30 km depth (Hansen et al., 2015) and its present-day temperature of ca. 850°C (Cipar et al., 2020) significantly higher than the temperature for a stable continental crust. The magmatic activity, which occurs in various volcanic fields along the rift, focused in two periods. The Oligo-Miocene stage is characterized by a silicic magmatic activity and caldera development (Cather, 1990; Chapin et al., 2004) in response to the melting of the 'hydrated' lithospheric mantle (Li et al., 2008; Sommer and Gauert, 2011; Rowe et al., 2015; Butcher et al., 2017) and lower crust metapelites below the rift. The crustal melting and mafic melt intrusions lead to a progressive granulitization (Padovani and Carter, 1977;

Cipar et al., 2020). Large granitic batholiths were emplaced in the upper crust modifying the heat budget (Morgan et al., 1986). This magmatic activity is contemporaneous of the 'ignimbrite flare-up 'in the Basin and Range (Best et al., 2013). It is followed by a volcanic lull between 25-15 Ma. This lull is coeval to the strain localization in the rift occurring between 20 and 15Ma. The second main volcanic stage, predominantly basaltic, spans from 10 Ma to the present-day (Chapin et al., 2004), with magmas source from the dry asthenospheric mantle. The magma is then predominantly emplaced as underplated bodies in the lower crust (Reiter et al., 2010) with basaltic vents at the surface (e.g., Taos plateau and East Potrillo volcanic fields).

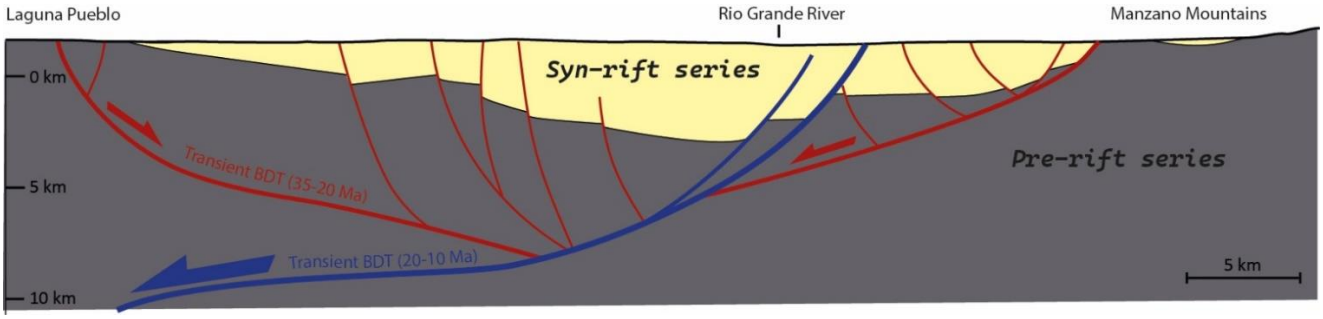

Figure 2: Crustal cross-section from the central part of the Albuquerque basin (see localization in figure 1) which highlights the two-stage rift evolution with a deepening of the brittle-ductile transition (BDT), based on seismic interpretations by Russell and Snelson (1994). The red faults are related to the first rift stage and the blue faults to the second rift stage.

The rift is composed of segments connected by linkage zones, which are characterized by fault trajectory bends. The following rift segments can be identified from south to north (**Figure 1**): Jornada del Muerto, Palomas, Tularosa, Albuquerque, San Luis, and Upper Arkansas. The main linkage zones include: the Rincon zone between the Jornada del Muerto and Palomas basins (Mack et al., 1994), the composite Socorro-Oviedo-Abbe-Springs zone between Tularosa/Palomas and Albuquerque, the oblique Española-Santo Domingo basin between Albuquerque and San Luis, and finally the Villa Grove accommodation zone (Chapin and Cather, 1994) between Upper Arkansas and San Luis. The main linkage zone is the Española-Santo Domingo basin, which forms a NE-SW elongated, diamond-shaped basin connecting the Albuquerque and San Luis rift segments. This linkage is the focus of the present work.

3. MODEL SET-UP

To analyze the structural evolution of the linkage zone of the Española-Santo Domingo basin, we modeled different configurations. At first order the rift linkage zones can be characterized by three parameters, the strike-perpendicular offset (x-offset) between rift segments, the along-strike offset (y-offset) and the strength of the continental crust (Neuhart et al., 2001), including the thickness of brittle crust and the role of ductile crust (strength ratio). Analogue modelling allows to simulate rift structures and their evolution through time. To model the brittle crust, whose behavior is of Mohr Coulomb type, we use dry sand layers (quartz sand MI 0.1/0.35 from Sibelco; average grain size 0.26 mm, friction angle ~32°, sand density ~1.55 g/cm3. The ductile layers are modelled using SGM-36 silicone, with a viscosity of 5×10^4 Pa·s at 20°C; a strain rate of 3×10^{-3} s^{-1} (Weijermars, 1986) and a density of 0.965 g/cm³. The impact of the ductile layer in the analogue models is quantified using a dimensionless number, the strength ratio R. It is adapted from the strength ratio of Bonnet, (1996). It is calculated as follows: $R = \frac{\int_{Hf}^{0}(\sigma_1-\sigma_3)_{brittle}}{\int_{Hd}^{0}(\sigma_1-\sigma_3)_{ductile}} = \frac{\rho g Hf}{2\eta UHd} L$ with L the width of the model, Hd and Hf the thickness of the brittle (sand) and ductile (silicone) layers, U the velocity and η the viscosity of the silicone.

These experiments are conducted on a large experimental (70cm) table above which a plexiglass or plastic plate is pre-cut into segments and rift linkage (Fig. 3). The displacement at 30 $cm.h^{-1}$ was generated and controlled by a computer driven stepper motor that pulled the plate at a constant rate (see Dall'Asta et al., 2024 for details).

We tested three setups varying scaling factors, rheology, and x- and y-offsets. The variations in scaling factors primarily affect the resolution of the deformation field analysis. Both rheological and offset variations were tested in an attempt to reproduce the deformation field observed in the Española-Santo Domingo basin. The model setups are summarized in Table 1. The MB2 model is a sand-only example with strong rheology, which is not suited to the case study but serves as a reference. The MB3 and MB4 models were developed by alternating silicone and sand to design a crust with a strong viscosity contrast between the lower and upper levels, as would likely be the case in the Rio Grande Rift. The x-offset and y-offset on the MB3 model is based on the spacing between the San Luis and Albuquerque basins (50 km) to reproduce the Espanola-Santo Domingo linkage zone with a weak rheology. The MB4 model is designed to reproduce late-rift linkage with a smaller x-offset (10 km), associated with the localization of deformation at the center of the rift segments.

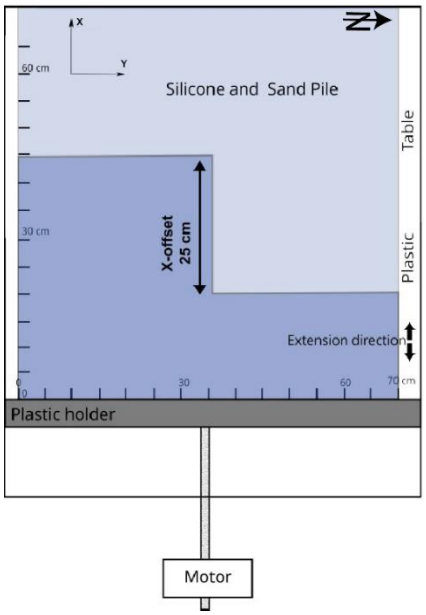

Figure 3: Map view of the experimental setup (Model MB3): only the dark blue area moves over the plastic plate positioned at the base of the model.

The models were extended by 5 cm to 12 cm. Model evolution was documented by laser acquisitions of the topography and top-down photos taken at each step, corresponding to 0.1 cm of extension for MB2 and MB4 and 0.2 cm of extension for MB3.The characteristics of the top-down photos and laser acquisitions are unchanged throughout the experiment. The photos have all been rectified in the same way than the initial one, which serves as a reference. The photos were processed using PivLab (Stamhuis and Thielicke, 2014) and Strainmap (Broerse et al., 2021) to extract the strain fields. The laser acquisition allowed to build digital elevation models (DEM) with a resolution of 1mm² (de Lavaissière et al., 2021).

Model	x-offset (cm)	y-offset (cm)/ obliquity (°)	Total Thickness (cm)	Sand thickness (cm)	Silicone thickness (cm)	Extension (cm)	Strength ratio (R)	x_h ratio	Scaling (Model vs Nature)	Type
MB2	15	4.1/20°	16	15	1	5.1	600	1	1cm=0.6km	Strong model/narrow offset
MB3	25	0/0°	6.2	5	1.2	12	66	5	1cm=2km	Weak model/large offset
MB4	5	4.19/50° and 0/0°	5.5	5	0.5	5	133	1	1cm=2km	Weak model/narrow offset

Table 1: Summary of analogue model characteristics. The x-offset and the x_h *ratio*, that correspond to the ratio between the *x*-offset and the thickness *h* of the brittle layer are key parameters for linkage zones as defined in Dall'Asta et al., (2024).

4. RESULTS

4.1 Espagnola-Santo Domingo basins

The Española-Santo Domingo basin (Figure 4) is oriented NE-SW and composed of a series of small graben and half-graben, buried beneath the late Tertiary and Quaternary volcano-sedimentary series (Figure 4). Early rift inactive basins are observed in the southern part of the Española-Santo Domingo basin and are commonly referred to as embayments (e.g., Hagan and Santa Fe embayment, Figure 4). Although part of the structure of these embayments is inherited from Laramide deformation , the modern shape of the embayments is related to early rift deformation (Lisenbee et al., 2013) as observed with the presence of early syn-rift sediments.

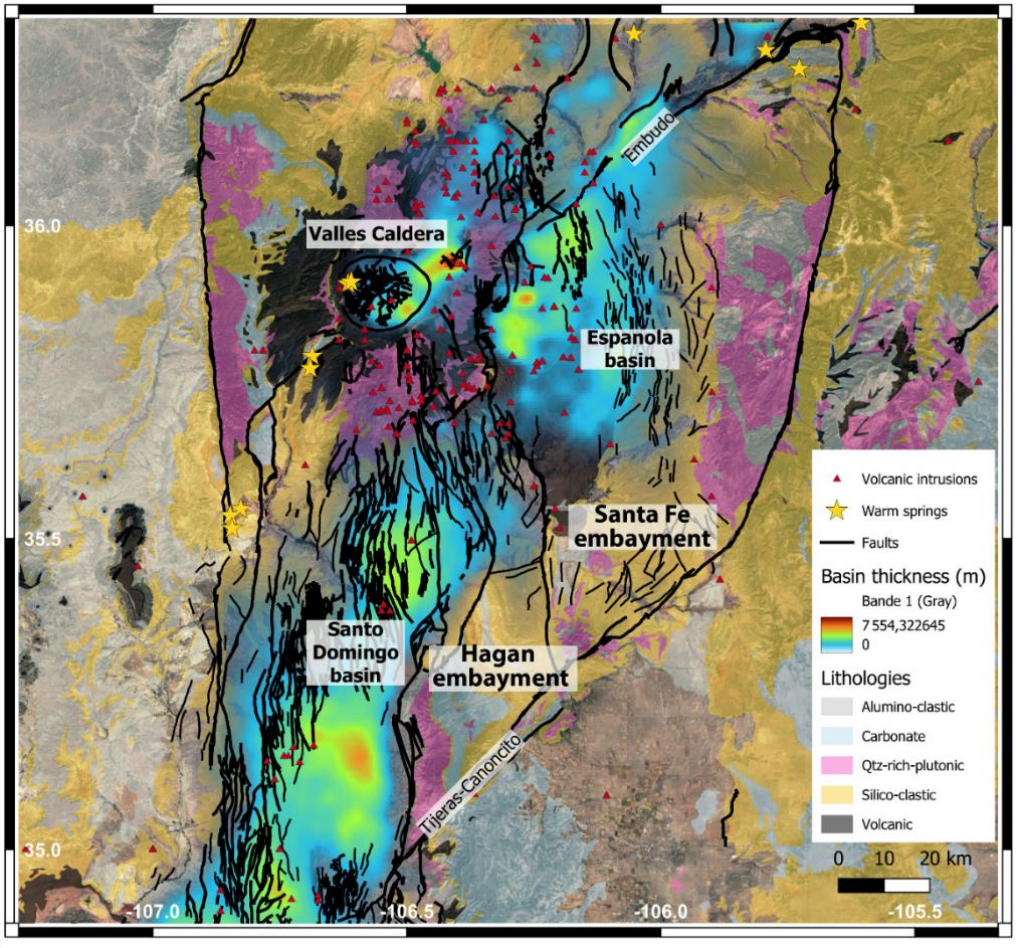

Figure 4: Map of the Española and Santo Domingo linkage with Quaternary faults (US Geological Survey, 2006 and Minor et al., 2013) and simplified lithological units. The basin thickness is from Grauch et al., (2013) showing localized depocenters of the Santa Fe Group. The volcanic intrusion data is from Carlson et al., (2001). The Qtz-rich plutonic lithological unit corresponds to the Proterozoic basement. The carbonate represents the Carboniferous pre-rift formations. Volcanic rocks range in age from the Tertiary to the present.

The basin is bounded to the north and south by the NE-SW trending Embudo and Tijeras fault systems, respectively (Fig. 4). The synthesis of slip data (Fig. 5) shows that syn-rift deformation is primarily accommodated in the basin by N-S trending faults, with secondary contributions from NE-SW faults. Furthermore, the traces of faults in the Santo-Domingo basin are concave and convex, indicating significant rotational component in the center of the linkage zone. In the late rift active basins, observed multi-scale en-echelon stair-like fault patterns can be related to the interaction between the two main fault sets. On a large -scale, those structures are related to the interaction between the Tijeras and Embudo faults and the N-S Rio Grande intra basin fault network. At the kilometric scale, multiple stair-like faults are observed in the Santo Domingo and Española domain (Figure 5). The kinematics in the basin faults is predominantly normal, although strike-slip component associated with oblique faults has been identified (Figure 5). These oblique faults have both dextral and sinistral shear with a major sinistral sense of shear (Minor et al., 2013).

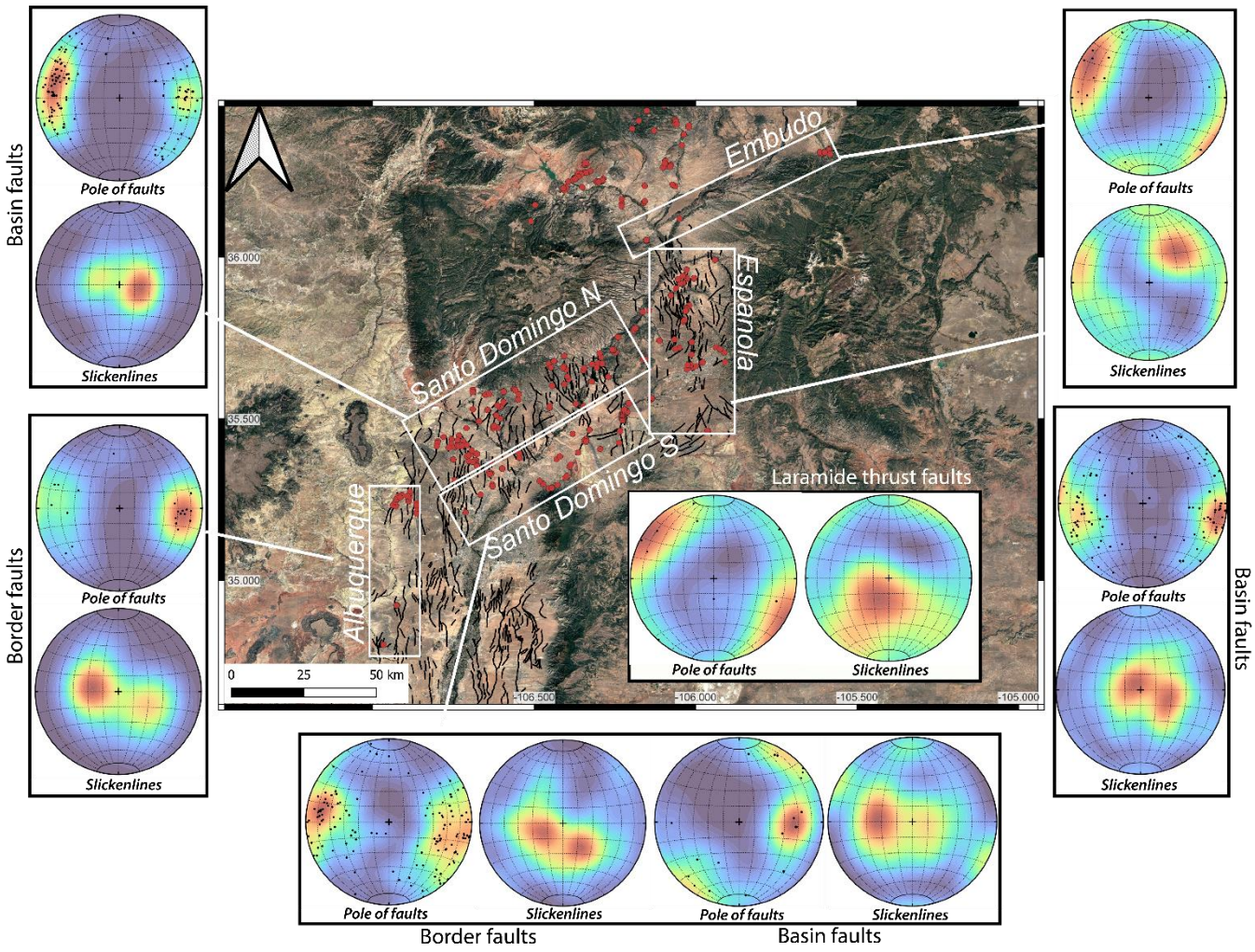

Figure 5: Synthesis of fault-slip data with pole of fault-planes (upper stereoplots) and slickenlines (lower stereoplots) from outcrops in the Española basin (Carter et al., 1995; Caine et al., 2017), the Santo Domingo basin (Minor et al., 2013; Liu et al., 2019), the Embudo fault (Bradford, 1992), and the Albuquerque basin (Liu et al., 2019). The red dots correspond to the slip data.

In order to better understand the rift evolution and to better calibrate the model setup, rheological profiles were calculated. The crustal composition and the geotherms are based on xenolith data from the work of Padovani and Carter (1977) and Cipar et al. (2020).

The lower crust underwent a change in composition throughout rifting by crustal melt and melt extraction under granulite facies conditions (**Error! Reference source not found.**A). This transformed the lower crust from high-grade metasediments to a mixt of mafic and felsic granulites. As mentioned by Cipar et al.,(2020), this represents a rare example of syn-rift granulitization, a process that could be more common than previously thought. The implication on the crustal rheology during extension are important. This shift in composition may have significantly impacted the rheology of the lower crust, potentially enhancing its resistance to deformation despite the elevated temperatures (**Error! Reference source not found.**B). Contrary to the model of Morgan et al. (1986), the most competent layer in our rheological profile is not the upper mantle but the mafic and felsic layered lower crust. This enhanced resistance might have facilitated the localization of deformation during the second rift stage. The increased of subsidence in the rift at ca. 15-10 Ma (van Wijk et al., 2018) could be a consequence of the strain localization and crustal necking. Nowadays, the lower crust and upper mantle show a weak behavior (**Error! Reference source not found.**C) as observed by Wilson et al. (2005);Hyndman (2017). This new change in the rheology of the crust explained by the occurrence of melt in the mantle and in the crust (Fu and Li, 2015; Feucht et al., 2019) weakening the lithosphere (Rushmer, 2001; Hyndman, 2017). The overall rheology of the crust is therefore weak, except for a brief period during which the crustal strength was higher, with a peak in resistance in the lower crust.

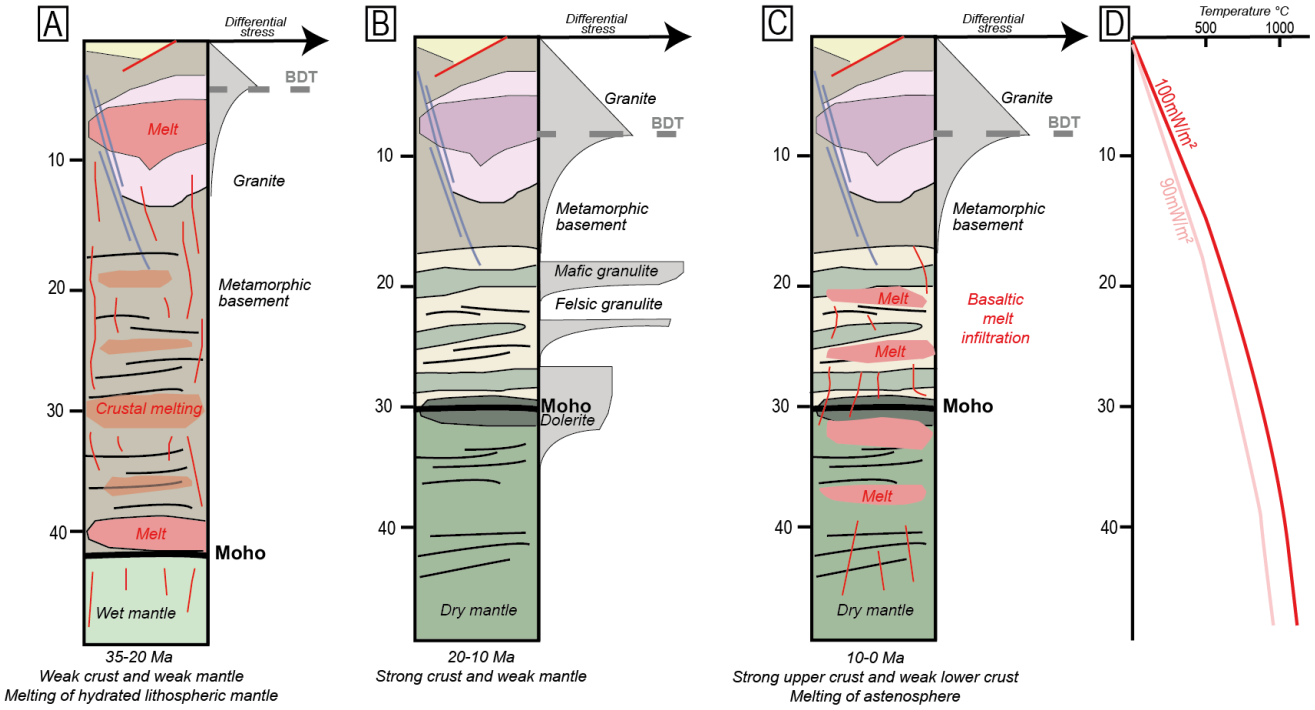

Figure 6: A- Lithological profile of the crust during the first rift stage (Oligo-Miocene) established based on the volcanic evolution and crustal xenoliths. Melting of the hydrated mantle and lower crust led to progressive granulitization of the lower crust and emplacement of large batholith in the upper crust. The rheological profile calculated assuming a heat flow of 100 mW/m², an integrated crustal-scale thermal gradient of 35°C/Km (Cipar et al., 2020) and a strain rate of 10^{-16} s^{-1} (Ricketts et al., 2014) shows a weak crustal and mantle behavior with a shallow Brittle-Ductile Transition (BDT) at ca. 5 km. B- Lithological profile during the second rift stage (Late Miocene) following granulitization of the crust. The rheological profile under a heat flow of 90 mW/m², a thermal gradient of ca. 28.5°C/Km (Cipar et al., 2020) and a strain rate of 10^{-16} s^{-1}. The profile was using Pikwitonei mafic granulite and Adironack felsic granulite (Burov and Watts, 2006). The BDT is at ca. 10 km depth. The lower crust shows strong behavior. C- Lithological profile during the second rift stage after melt infiltration. The rheology of the lower crust is weak due to the melt fraction. D- Thermal gradient used for rheological profiles

4.1. Analogue modelling

The MB2 model, composed solely of sand and therefore with strong rheology, shows the formation of a 20 cm-wide, oblique, left-lateral accommodation zone between two rift segments (Figure). The deformation is characterized by the stability in fault localization through time. At the first increments of extension, six major faults have formed: three west-verging faults in the eastern part of the experiment and three east-verging faults in the western part. Two of the most westernmost, east-verging faults have a N30°E orientation, which is parallel to the linkage zone cut into the plastic sheet. The other four faults are oriented N-S, perpendicular to the displacement direction. The interaction between faults with opposite vergence mimics the formation of an en-echelon rift, with a right-lateral shift. Conversely, the interaction between faults with identical vergence leads to the formation of relay ramps along major border faults as well as secondary faults in the basin.

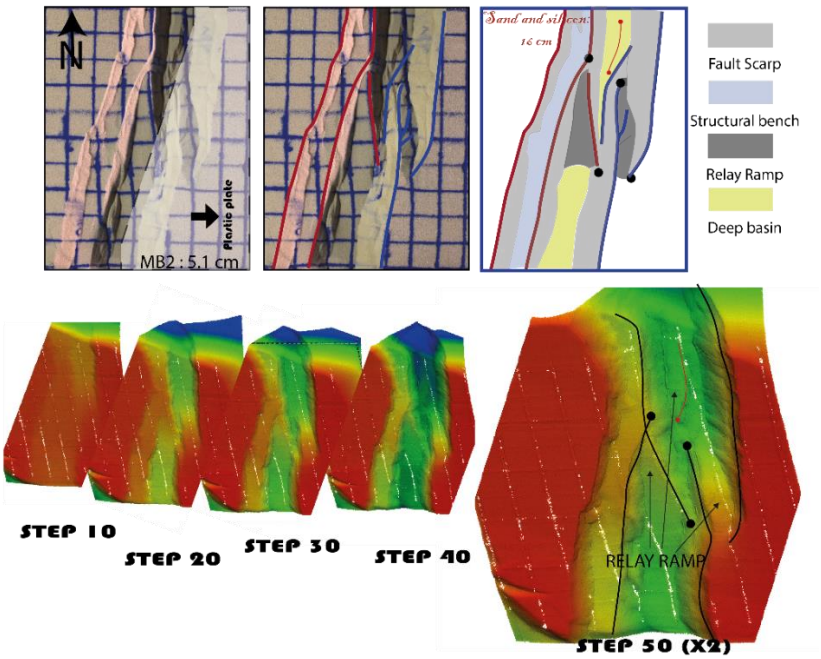

Figure 7: Results illustrating the formation of relay ramps from the MB2 analogue experiment. The uppermost panels correspond to interpreted top-down photographs of the model after 5.1cm of extension. The blue lines correspond to west-dipping faults, and the red lines correspond to east-dipping faults, respectively. The lowermost panels correspond to sequence of laser images (low relief=blue/green, high relief=red), every ten steps (1 step correspond to 0.1 cm of extension). Note scale exaggeration x2 for the last step, which is structurally interpreted.

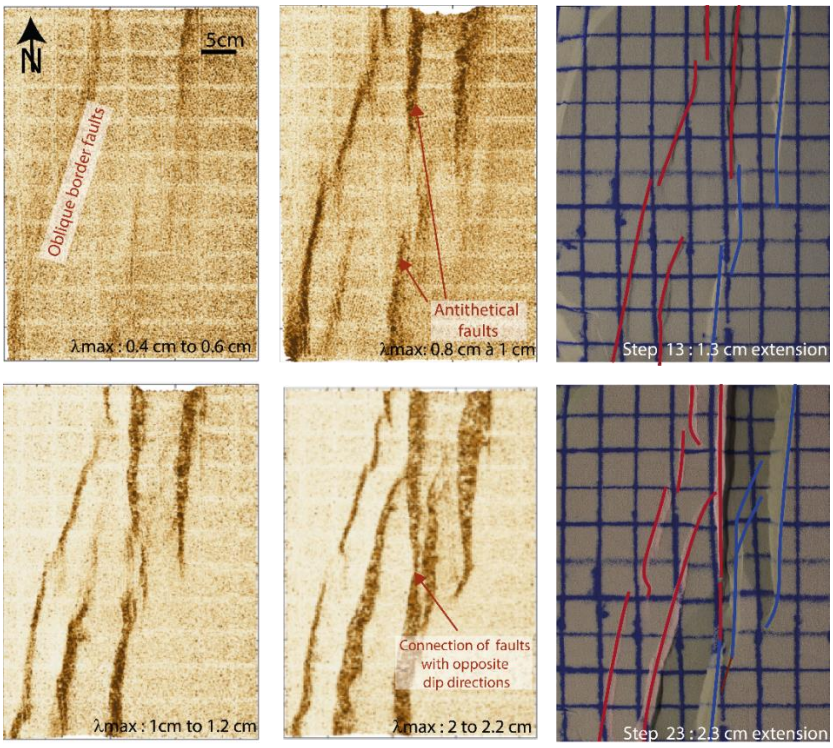

Figure 8: Results from the MB2 analogue experiment. The 4 images on the left illustrate the evolution of the parameter λmax, the principal strain axis (λmax=1 indicates no length change). In these images, λmax ranges from 10 in the darkest areas to 1 in the lightest areas. The 2 images on the right are interpreted top-down photos at 1.3 et 2.3 cm of extension.

Using PIVLAB and STRAINMAP image analysis software, we visualize the evolution of deformation over time (Fig. 8). This analysis allows to examine the connection of faults with opposite vergence in an accommodation zone. The model demonstrates that such a connection is possible but mechanically unstable, as it becomes visible at 2 cm of extension and then disappears at the next increment.

The MB4 model, with alternating layers of silicone and sand and associated with a less resistant rheology than the MB2 model, simulates the formation of a localized (narrow) rift with two 10 cm-wide accommodation zones. These zones are characterized by faults forming sequentially basinward (Figure 9: Surface evolution from laser acquisitions of MB4 (low relief= green, high relief=red) at 2 cm (left panel) and 4 cm extension (rigth panel). The blue lines correspond to west-dipping faults, and the red lines correspond to east-dipping faults, respectively.

). The accommodation zone on the north side of the model, which develops over the oblique cut in the basal plastic, is characterized by the formation of en-echelon fault scarps associated with left-lateral movement. The accommodation zone on the south side of the model, which develops over the orthogonal cut in the basal plastic, is characterized by the development of relay zones between rectilinear faults. It should be noted that in the southern part of the model, a perched basin, or structural bench, forms as the stretched area widens.

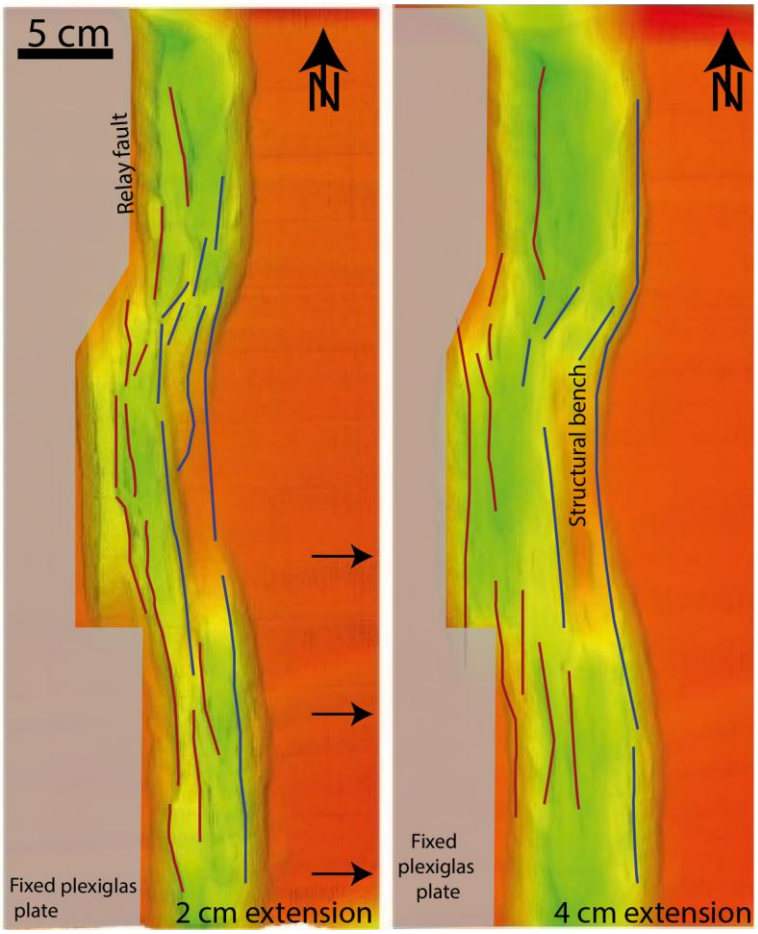

Figure 9: Surface evolution from laser acquisitions of MB4 (low relief= green, high relief=red) at 2 cm (left panel) and 4 cm extension (rigth panel). The blue lines correspond to west-dipping faults, and the red lines correspond to east-dipping faults, respectively.

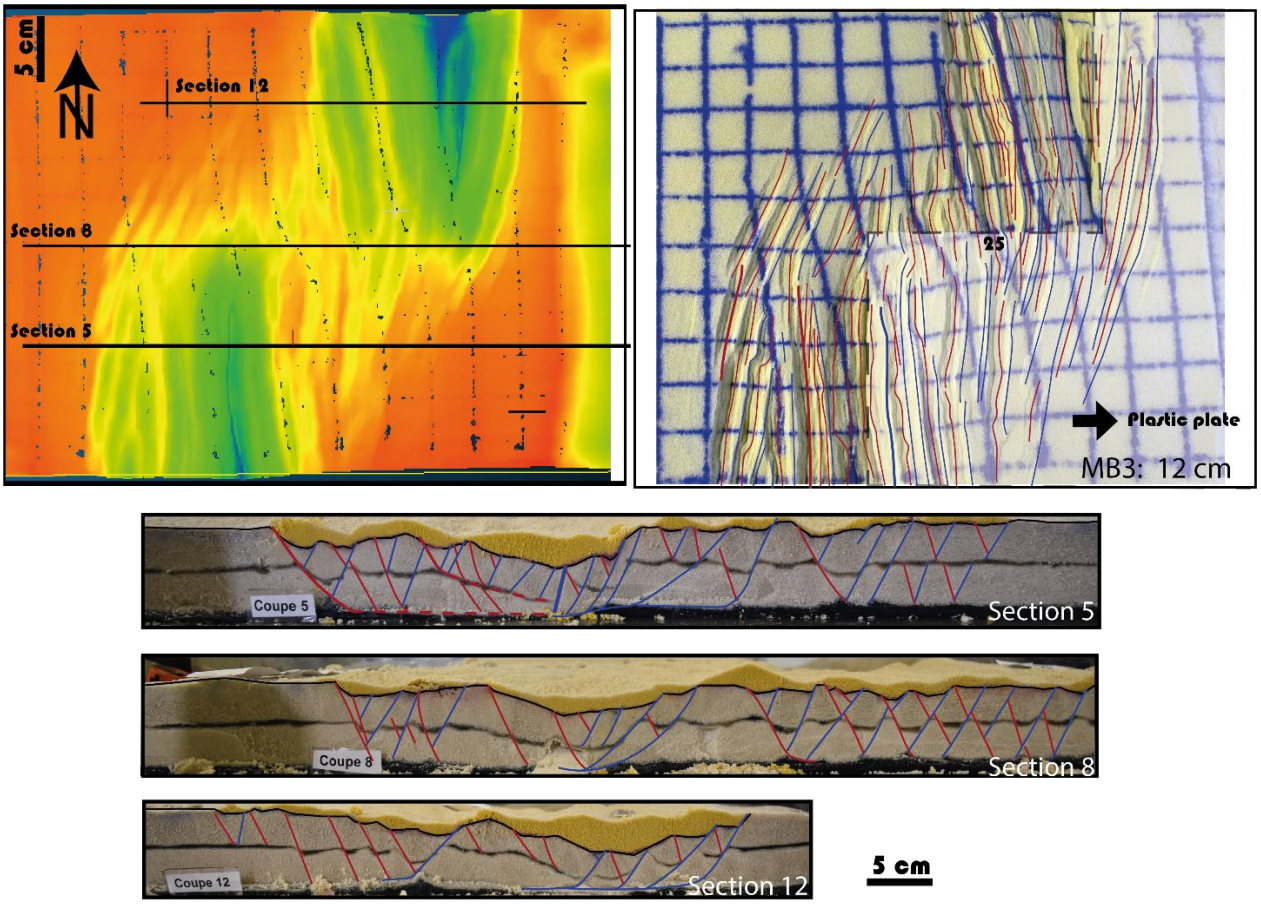

Figure 10: Results of the MB3 analogue experiment. The 2 images on the top represent respectively (i) a spatial distribution of Z at step 60 (i.e. 12 cm extension) from the laser acquisitions (low relief= green, high relief=red); (ii) an interpreted top-down photograph of the experiment at step 60. The blue lines correspond to west-dipping faults, and the red lines correspond to east-dipping faults, respectively. The cross-sections in the main segments and in the linkage highlight the fault pattern at the end of the experiment.

The MB3 model consisting of alternating layers of silicone and sand with a rheology weaker than MB4. It shows the formation of distributed rift (i.e. wide rift) with succession of horsts and grabens, with two major grabens to the east and west, separated by a 40 cm wide sinistral accommodation zone (Figure). The model is characterized by the distribution of faults (Figure), which develop sequentially with progressive widening of the thinned area.

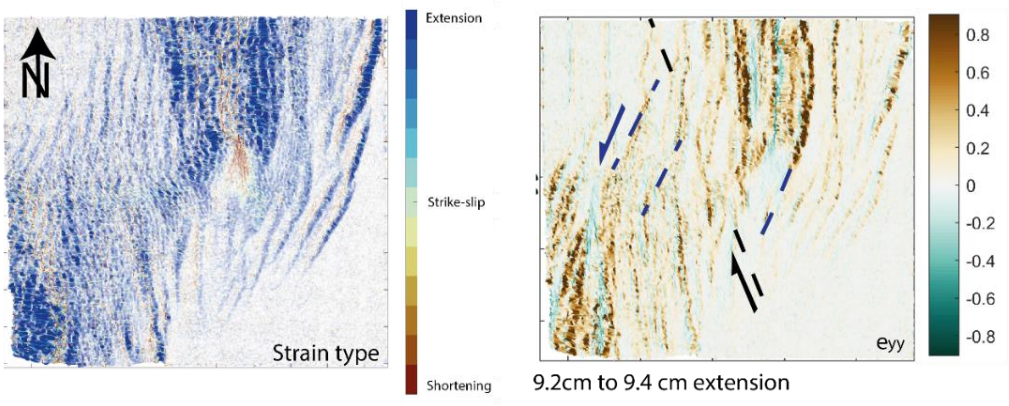

Figure 11: Strain type and εyy (between -0.5 for the greenest zones and 0.5 for the brownest zones) extracted from the STRAINMAP software between steps 46 and 48 (i.e. 9.2 and 9.6 cm of extension), showing possible conjugate faults with a dextral component.

STRAINMAP analysis highlights the presence of second-order structures oriented N60 to N70°E (Fig. 11). These structures, not clearly visible in the photographs, may correspond to conjugate faults with normal dextral kinematics, related to the N110°E-oriented fault system with normal sinistral kinematics.

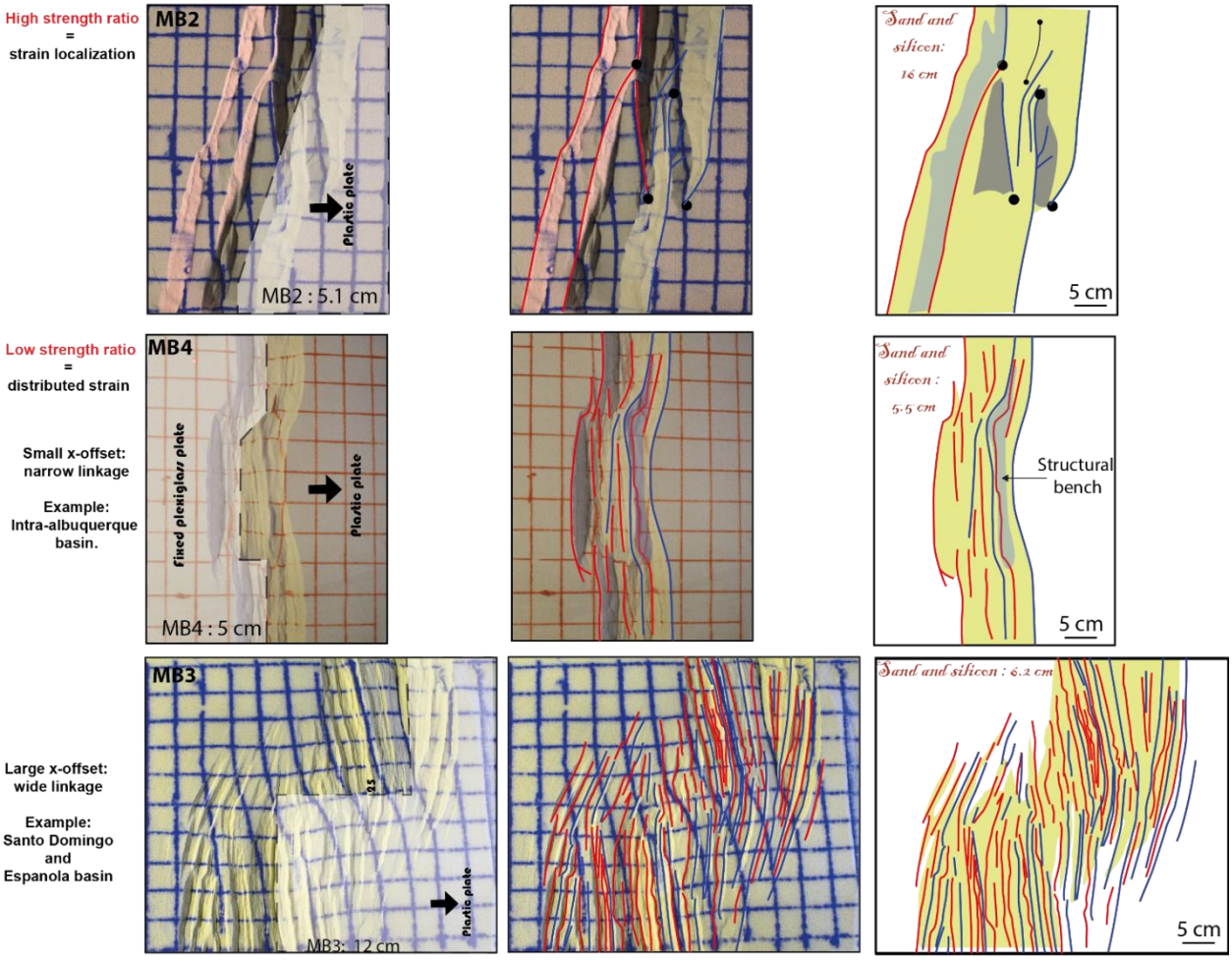

Figure 12: Synthesis of the models with various strength ratios and x- and y-offsets. Top views and their interpretation. Blue lines and green lines stand for fault dipping, respectively, to the south or to the north.

The comparison of the three models highlighted that the model with high strength ratio (MB2, Strength ratio R = 600) shows a high degree of strain localization, which remains stable despite the increase in strain (Fig. 12). In contrast, models with lower strength ratios (XP MB3, R = 66 and MB4, R = 133) show a wider distribution of faults, with newly formed faults emerging as strain increases. Also, the three models suggest that the width of the rift domain mainly depends on the X-offset (Fig. 12).

5. DISCUSSION

5.1 Comparison between the analogue models and the Española-Santa Domingo basin

At first order, the analogue model MB3 replicates the large-scale diamond-shaped geometry and the fault trajectories observed in the Española-Santo Domingo basin (Fig. 13).

The detailed strain field of the Española-Santo Domingo linkage zone can be explained using both the weak model with a large offset (MB3) for the first rift stage, and the weak model with a narrow offset for the second rift stage (MB4). The weak model with a large offset helps to explain the general kinematics of the Española basin, with deformation distributed in various basin-bounding faults (Fig. 12). The linkage zone in the MB3 model is composed of numerous N-S to NE-SW sub-basins, akin to those observed in the Española-Santo Domingo basin. The overlap of the two rift segments results in a rotation of the segment tips towards a NE-SW direction. The segment tips, exhibiting obliquity of around 20-30° and minimal deformation, bear a resemblance to the embayment observed in the Española-Santo Domingo basins. The central region of the linkage basin shows a pronounced rotational strain forming convex and concave fault similar to those observed in the Española-Santo Domingo basin. The model successfully replicates the strike-slip component within the

border faults of the border of the linkage, characterized by a substantial sinistral shear along the linkage as observed along the Embudo fault (Fig.5).

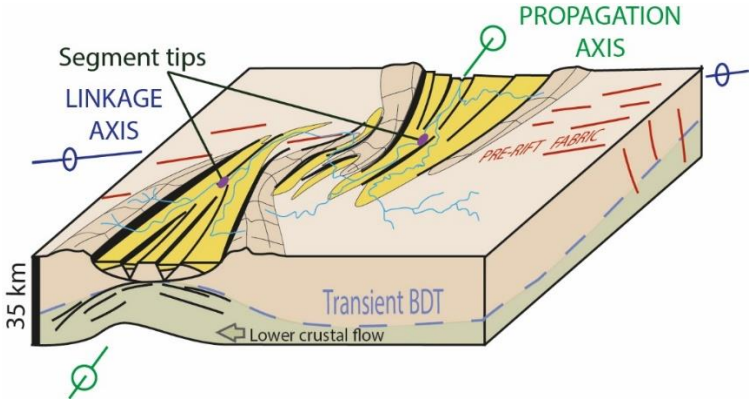

Figure 13: Block diagram illustrating the structural characteristics of a broad accommodation zone, specifically focusing on the linkage zone between the Española Basin and the Santo Domingo Basin. This diagram highlights the key structures within the linkage zone and emphasizes the influence of inherited structures. BDT: Brittle-Ductile Transition.

In contrast, the weak model MB2 with a narrow offset reproduces a stair-like fault pattern, with a more localized deformation. A major difference between the case study and the models is the Embudo and Tijeras transfer faults, which are not reproduced in the models.

5.2 The role of inheritance

Two main Proterozoic lineaments can be observed in the central Rio Grande rift domain. These lineaments are oriented NE-SW and N-S, and correspond to the border faults of the diamond-shaped Española-Santo Domingo Basin, highlighting the pivotal role of structural inheritance. The x-offset between rift segments appears to be controlled by the N-S Proterozoic lineaments (Marshak et al., 2000) that were reactivated throughout the Phanerozoic and correspond to major weakness zones (Figure). The y-offset seems to be controlled by the NE-SW Jemez lineament related to a Proterozoic suture between the Yavapai and Mazatzal terranes.

Some structures appear to have been reactivated during rifting, including the Embudo and Tijeras transfer faults, identified as inherited Laramide structures (Woodward, 1984; Sims et al., 2002; Lisenbee et al., 2013). Based on the ratio between the x-offset and the thickness h of the brittle layer, the linkage type developed in the MB3 model falls at the boundary between oblique linkage and transfer zone types, which differ in their degree of deformation localization (Dall'Asta et al., 2024). We propose that the Embudo and Tijeras faults demonstrate the localization of strike-slip deformation within the large sinistral accommodation zone between rift segments, driven by structural inheritance.

Based on rheological profiles, the thermal evolution and the compositional inheritance exerted a substantial influence on the geometry of linkage, with elevated thermal gradient and Moho temperature favoring a weak lower crust behavior and lower crust flow. The elevated temperature in the lower crust throughout extensional event led to distributed deformation, thereby weakening the crustal behavior and resulting in a broad linkage zone, as observed during the first rift stage.

5.3 Implications for geothermal exploration

Within the Española basin, warm springs are observed at the intersection between the N-S and NE-SW oriented fault, particularly in proximity to the Embudo fault. These springs are localized within the Proterozoic basement, a region of significant geologic interest for geothermal exploration. Hidden hydrothermal systems potentially exists beneath the syn-rift cover at these specific intersections, a possibility worth investigating.

The linkage zones have a significant impact on the circulation of fluids (both melted and aqueous) within the crust (Rowland and Sibson, 2004; Lupi et al., 2010; Faulds and Hinz, 2015). In the main segments, faults are predominantly rift-parallel, exhibiting a predominant normal regime. This configuration tends to restrict major fault intersections and accommodation zones. Conversely, within the linkage zones, the fault distribution is more intricate, with at least interacting two fault directions, multiple fault intersections and thereby enhancing the permeability of the crust. The analysis of finite strain during extension reveals that the maximum strain is observed within the linkage zone. Assuming that the total strain is proportional to the fracture density and bulk permeability, it can be concluded that the linkage zones are the most favorable location for high permeability within the rift. Furthermore, the strain in the linkage zone exhibits a pronounced rotational component, thereby further enhancing the bulk permeability.

Previous works based on analogue modelling shows that along-axis magma migration tend to concentrate melt in the linkage zones (Corti et al., 2003). This is due to a pressure decrease in the linkage in response to oblique faults. The shear wave velocity model along the Rio Grande rift from Fu and Li (2015) allows to image the melt fraction within the crust. While the shear waves anomalies are widespread

below the rift in the upper mantle, the anomalies are focused along the rift linkage zone in the upper crust, starting with the Española basin where negative anomalies are observed throughout the crust.

In terms of aqueous fluids, the significant permeability increase expected in the linkage zone favors fracture and fault-controlled hydrothermal systems. As demonstrated by Williams et al., (2008), various convective systems have been identified in New Mexico along the Rio Grande rift. The main systems are located in the Española basin, the Socorro basins and the area around Rincon. They correspond to rift linkage zones with various x-offset and y-offset highlighting the key role played by those structures. However, the impact of the different linkage offset on the behavior of the hydrothermal systems requires further investigations, in particular, the linkage zones provide second and third order structural settings with strong interest for localized fluid flow which have to be further characterized.

The findings from the Rio Grande rift, particularly those pertaining to the linkage zone and its implications for fluid transfer, can be extrapolated to analogous rift systems, such as the East African rift, or to the Great Basin. Furthermore, the rheological evolution of the crust and mantle in response to strain and magmatic activity exhibits significant parallels between the Rio Grande rift and the Great Basin.

REFERENCES

Best, M.G., Gromme, Sherman., Deino, A.L., Christiansen, E.H., Hart, G.L., Tingey, D.G., 2013. The 36–18 Ma Central Nevada ignimbrite field and calderas, Great Basin, USA: Multicyclic super-eruptions. Geosphere 9, 1562–1636. https://doi.org/10.1130/GES00945.1

Bonnet, E., 1996. Localisation de la déformation dans les milieux fragile-ductile: approche expérimentale et application à la lithosphère continentale. Mémoire de Géosciences-Rennes n°81, 183 p., ISBN : 2-905534-80-7

Bradford, S.C., 1992. Kinematics of an accommodation zone in the Rio Grande rift: the Embudo fault zone, northern New Mexico. The Ohio State University.

Broerse, T., Krstekanić, N., Kasbergen, C., Willingshofer, E., 2021. Mapping and classifying large deformation from digital imagery: application to analogue models of lithosphere deformation. Geophys. J. Int. 226, 984–1017.

Burov, E.B., Watts, A.B., 2006. The long-term strength of continental lithosphere:" jelly sandwich" or" crème brûlée"? GSA Today 16, 4.

Butcher, L.A., Mahan, K.H., Allaz, J.M., 2017. Late Cretaceous crustal hydration in the Colorado Plateau, USA, from xenolith petrology and monazite geochronology. Lithosphere 9, 561–578. https://doi.org/10.1130/L583.1

Caine, J.S., Minor, S.A., Grauch, V.J.S., Budahn, J.R., Keren, T.T., 2017. A comprehensive survey of faults, breccias, and fractures in and flanking the eastern Española Basin, Rio Grande rift, New Mexico. Geosphere 13, 1566–1609. https://doi.org/10.1130/GES01348.1

Carlson, R.W., Walker, D., Black, R., Glazner, A., Farmer, L., Grossman, J., 2001. NAVDAT: A western North American volcanic and intrusive rock geochemical database, in: Geological Society of America Abstracts with Programs. p. 175.

Carter, K.E., Gardner, J.N., Bauer, P.W., 1995. Quaternary fault kinematics in the northwestern Española basin, Rio Grande rift, New Mexico, in: Geology of the Santa Fe Region, Field Conf. Guideb. NM Geol. Soc., 46th. pp. 97–102.

Cather, S.M., 1990. Stress and volcanism in the northern Mogollon-Datil volcanic field, New Mexico: Effects of the post-Laramide tectonic transition. GSA Bull. 102, 1447–1458. https://doi.org/10.1130/0016-7606(1990)102<1447:SAVITN>2.3.CO;2

Chapin, C.E., Cather, S.M., Keller, G.R., 1994. Tectonic setting of the axial basins of the northern and central Rio Grande rift. Spec. Pap.-Geol. Soc. Am. 5–5.

Chapin, C.E., Wilks, M., McIntosh, W.C., Cather, S.M., Kelley, S.A., 2004. Space-time patterns of Late Cretaceous to present magmatism in New Mexico—Comparison with Andean volcanism and potential for future volcanism. N. M. Bur. Geol. Miner. Resour. Bull. 160, 13–40.

Cipar, J.H., Garber, J.M., Kylander-Clark, A.R., Smye, A.J., 2020. Active crustal differentiation beneath the Rio Grande Rift. Nat. Geosci. 13, 758–763.

Corti, G., Bonini, M., Conticelli, S., Innocenti, F., Manetti, P., Sokoutis, D., 2003. Analogue modelling of continental extension: a review focused on the relations between the patterns of deformation and the presence of magma. Earth-Sci. Rev. 63, 169–247.

Dall'Asta, N., Denèle, Y., Regard, V., Frayssignes, A., Hoareau, G., Leroy, S., Pires, T., 2024a. Analogue model of rift linkage and inversion with application to the Western Alps. Comptes Rendus Géoscience 356, 1–21.

Dall'Asta, N., Denèle, Y., Regard, V., Frayssignes, A., Hoareau, G., Leroy, S., Pires, T., 2024b. Analogue model of rift linkage and inversion with application to the Western Alps. Comptes Rendus Géoscience 356, 1–21.

Daniel, C.G., Karlstrom, K.E., Williams, M.L., Pedrick, J.N., Bauer, P.W., Kues, B.S., Dunbar, N.W., 1995. The reconstruction of a middle Proterozoic orogenic belt in north-central New Mexico, USA. N. M. Geol. Soc. Guideb. 46, 193–200.

de Lavaissière, L., Bonnet, S., Guyez, A., Davy, P., 2021. Generation of autogenic knickpoints in laboratory landscape experiments evolving under constant forcing. Earth Surf. Dyn. Discuss. 2021, 1–31.

Faulds, J., Hinz, N., 2015. Favorable tectonic and structural settings of geothermal systems in the Great Basin region, western USA: Proxies for discovering blind geothermal systems, in: Proceedings World Geothermal Congress, Melbourne, Australia, 19-25 April 2015. Nevada Bureau of Mines and Geology, University of Nevada, Reno.

Feucht, D.W., Bedrosian, P.A., Sheehan, A.F., 2019. Lithospheric signature of late Cenozoic extension in electrical resistivity structure of the Rio Grande rift, New Mexico, USA. J. Geophys. Res. Solid Earth 124, 2331–2351.

Fu, Y.V., Li, A., 2015. Crustal shear wave velocity and radial anisotropy beneath the Rio Grande rift from ambient noise tomography. J. Geophys. Res. Solid Earth 120, 1005–1019.

Grauch, V.J.S., Connell, S.D., Hudson, M.R., 2013. New perspectives on the geometry of the Albuquerque Basin, Rio Grande rift, New Mexico: Insights from geophysical models of rift-fill thickness. New Perspect. Rio Gd. Rift Basins Tecton. Groundw. Geol. Soc. Am. Spec. Pap. 494, 427–462.

Hansen, S.M., Dueker, K., Schmandt, B., 2015. Thermal classification of lithospheric discontinuities beneath USArray. Earth Planet. Sci. Lett. 431, 36–47. https://doi.org/10.1016/j.epsl.2015.09.009

Hyndman, R.D., 2017. Lower-crustal flow and detachment in the North American Cordillera: a consequence of Cordillera-wide high temperatures. Geophys. J. Int. 209, 1779–1799.

Li, Z.-X.A., Lee, C.-T.A., Peslier, A.H., Lenardic, A., Mackwell, S.J., 2008. Water contents in mantle xenoliths from the Colorado Plateau and vicinity: Implications for the mantle rheology and hydration-induced thinning of continental lithosphere. J. Geophys. Res. Solid Earth 113. https://doi.org/10.1029/2007JB005540

Lisenbee, A.L., Hudson, M.R., Grauch, V.J.S., 2013. Multi-stage Laramide deformation in the area of the southern Santa Fe embayment (Rio Grande rift), north-central New Mexico. Geol. Soc. Am. Spec. Pap. 494, 239–260.

Liu, Y.A., Murphy, M.A., van Wijk, J., Koning, D.J., Smith, T., Andrea, R.A., 2019. Progressive opening of the northern Rio Grande rift based on fault structure and kinematics of the Tusas-Abiquiu segment in north-central New Mexico, U.S. Tectonophysics 753, 15–35. https://doi.org/10.1016/j.tecto.2019.01.004

Lupi, M., Geiger, S., Graham, C.M., 2010. Hydrothermal fluid flow within a tectonically active rift-ridge transform junction: Tjörnes Fracture Zone, Iceland. J. Geophys. Res. Solid Earth 115.

Minor, S.A., Hudson, M.R., Caine, J.S., Thompson, R.A., Grauch, V.J.S., 2013. Oblique transfer of extensional strain between basins of the middle Rio Grande rift, New Mexico: Fault kinematic and paleostress constraints. New Perspect. Rio Gd. Rift Basins Tecton. Groundw. Geol. Soc. Am. Spec. Pap. 494, 345–382.

Morgan, P., Seager, W.R., Golombek, M.P., 1986. Cenozoic thermal, mechanical and tectonic evolution of the Rio Grande rift. J. Geophys. Res. Solid Earth 91, 6263–6276.

Olsen, K.H., Scott Baldridge, W., Callender, J.F., 1987. Rio Grande rift: An overview. Cont. Rifts-Princ. Reg. Charact. 143, 119–139. https://doi.org/10.1016/0040-1951(87)90083-7

Padovani, E.R., Carter, J.L., 1977. Aspects of the Deep Crustal Evolution Beneath South Central New Mexico, in: The Earth's Crust, Geophysical Monograph Series. pp. 19–55. https://doi.org/10.1029/GM020p0019

Reiter, M., Chamberlin, R.M., Love, D.W., 2010. New data reflect on the thermal antiquity of the Socorro magma body locale, Rio Grande Rift, New Mexico. Lithosphere 2, 447–453. https://doi.org/10.1130/L115.1

Ricketts, J.W., Karlstrom, K.E., Priewisch, A., Crossey, L.J., Polyak, V.J., Asmerom, Y., 2014. Quaternary extension in the Rio Grande rift at elevated strain rates recorded in travertine deposits, central New Mexico. Lithosphere 6, 3–16. https://doi.org/10.1130/L278.1

Ricketts, J.W., Kelley, S.A., Karlstrom, K.E., Schmandt, B., Donahue, M.S., van Wijk, J., 2016. Synchronous opening of the Rio Grande rift along its entire length at 25–10 Ma supported by apatite (U-Th)/He and fission-track thermochronology, and evaluation of possible driving mechanisms. GSA Bull. 128, 397–424. https://doi.org/10.1130/B31223.1

Rowe, M.C., Lassiter, J.C., Goff, K., 2015. Basalt volatile fluctuations during continental rifting: An example from the R io G rande R ift, USA. Geochem. Geophys. Geosystems 16, 1254–1273.

Rowland, J.V., Sibson, R.H., 2004. Structural controls on hydrothermal flow in a segmented rift system, Taupo Volcanic Zone, New Zealand. Geofluids 4, 259–283.

Rushmer, T., 2001. Volume change during partial melting reactions: implications for melt extraction, melt geochemistry and crustal rheology. Partial Melting Crust Flow Orogens 342, 389–405. https://doi.org/10.1016/S0040-1951(01)00172-X

Russell, L.R., Snelson, S., 1994. Structure and tectonics of the Albuquerque Basin segment of the Rio Grande rift: Insights from reflection seismic data. Geol. Soc. Am. Spec. Pap. 291, 83–112.

Sims, P.K., Stein, H.J., Finn, C.A., 2002. New Mexico structural zone—an analogue of the Colorado mineral belt. Deep Crustal Controls Miner. Trends 21, 211–225. https://doi.org/10.1016/S0169-1368(02)00090-2

Sommer, H., Gauert, C., 2011. Hydrating laterally extensive regions of continental lithosphere by flat subduction: A pilot study from the North American Cordillera. J. Geodyn. 51, 17–24.

Stamhuis, E., Thielicke, W., 2014. PIVlab–towards user-friendly, affordable and accurate digital particle image velocimetry in MATLAB. J. Open Res. Softw. 2, 30.

van Wijk, J., Koning, D., Axen, G., Coblentz, D., Gragg, E., Sion, B., 2018. Tectonic subsidence, geoid analysis, and the Miocene-Pliocene unconformity in the Rio Grande rift, southwestern United States: Implications for mantle upwelling as a driving force for rift opening. Geosphere 14, 684–709. https://doi.org/10.1130/GES01522.1

Weijermars, R., 1986. Flow behaviour and physical chemistry of bouncing putties and related polymers in view of tectonic laboratory applications. Tectonophysics 124, 325–358.

Williams, C.F., Reed, M.J., Mariner, R.H., DeAngelo, J., Galanis, S.P., 2008. Assessment of moderate-and high-temperature geothermal resources of the United States. Geological Survey (US).

Wilson, D., Aster, R., West, M., Ni, J., Grand, S., Gao, W., Baldridge, W.S., Semken, S., Patel, P., 2005. Lithospheric structure of the Rio Grande rift. Nature 433, 851–855.

Woodward, L.A., 1984. Basement control of Tertiary intrusions and associated mineral deposits along Tijeras-Cañoncito fault system, New Mexico. Geology 12, 531–533. https://doi.org/10.1130/0091-7613(1984)12<531:BCOTIA>2.0.CO;2

Zwaan, F., Schreurs, G., 2017. How oblique extension and structural inheritance influence rift segment interaction: Insights from 4D analog models. Interpretation 5, SD119–SD138.